

Projections of ocean wave heights - climate change signal and Uncertainty

Xiaolan L. Wang and Val R. Swail

Climate Research Branch, Meteorological Service of Canada, Downsview, Ontario

1. INTRODUCTION

Changes in the Earth's climate occur as a result of both internal variability within the climate system and external factors. The external factors can be anthropogenic or natural. The increasing concentration of atmospheric greenhouse-gases (GHG; due to anthropogenic emissions) tends to warm the Earth's surface and lower atmosphere, while an increase in some types of aerosols tends to cool them. Natural factors, such as changes in solar output or explosive volcanic activity, can also cause radiative forcing and hence influence the Earth's climate.

Complex physically-based climate models are required to provide detailed estimates of feedbacks and regional features in the climate system. Although confidence in the ability of these models to provide useful projections of future climate has improved due to their demonstrated performance on a range of space and time-scales, the present-day climate models cannot yet simulate all aspects of climate (Houghton et al. 2001). For example, there are particular uncertainties associated with clouds and their interaction with radiation and aerosols.

Actually, there are several levels of uncertainty in the generation of "regional" climate change information [including generation of parameters/elements that are not directly available from the output of Atmosphere-Ocean General Circulation Models (AOGCMs), such as ocean wave heights]. The first level of uncertainty is associated with alternative scenarios of future emissions, their conversion to atmospheric concentrations and the radiative effects of these. The second level of uncertainty is related to the simulation of the transient climate response by AOGCMs for a given emission scenario. The final level of uncertainty occurs when the AOGCM data are used to generate "regional" climate change information. In this regard, uncertainties are associated with imperfect knowledge and/or representation of physical processes, limitations due to the numerical approximation, simplification and assumptions in the models and/or approaches, internal model variability, and inter-model or inter-method differences in the simulation of climate response to given forcing conditions (Houghton et al. 2001).

Besides, climate model simulations are a combination of a forced climate change component together with internally generated natural variability. The internal variability of the global and regional climate system adds a further level of uncertainty in the evaluation of a climate change simulation.

As an important element of the climate system, ocean wave heights (among many other ocean surface characteristics) could be affected by anthropogenic forcing. However, ocean wave heights are not directly available from the output of global climate models. Useful projections of future wave height climate need to be produced through dynamical or statistical "downscaling" approaches, just like other regional climate change information. Therefore, there are various sources of uncertainty in the generation of ocean wave height climate change projections. Using the Canadian coupled climate model, CGCM2, projections of future climate with the IPCC IS92a and the SRES (Special Report on Emissions Scenarios; Nakicenovic and Swart 2000) A2 and B2 forcing scenarios, Wang and Swail (2004) and Wang et al. (2004a) produced ocean wave climate change scenarios for the northern hemisphere oceans for the 21st century. Their results show that significant changes can be anticipated in both the North Atlantic and the North Pacific under all the three forcing scenarios. The rate and sign of the projected future wave height changes are not constant throughout the century; and in some regions, these appear to be quite dependant on the forcing conditions. The rate of change appears to have a positive relationship with the rate of increase in the GHG forcing (Wang and Swail 2004). These among-scenarios differences lie within the first level of uncertainty mentioned above. The existence of these various sources of uncertainty requires us to characterize the uncertainty, to evaluate the level of confidence in a "regional" climate change simulation.

One of the criteria to evaluate the level of confidence in a "regional" climate change simulation can be based on how well the climate change simulations converge across models and methods (Houghton et al. 2001). Aiming to characterize the various levels of uncertainty, to provide a better estimate of the projected climate change of ocean wave heights, this study made and analyzed projections of ocean wave heights using projections of future climate conducted with three coupled AOGCMs: the Canadian CGCM2 (Flato and Boer, 2001), the Hadley Centre's HadCM3 (Gordon et al. 2000), and the German ECHAM4 (Roeckner et al. 1996a and 1996b). For each of the three forcing scenarios (i.e., IS92a, A2, and B2), three integrations were run with the CGCM2, but only one integration was run with each of the other two models. The projections of ocean wave heights were then subject to ANOVA (Analysis of Variance) analyses to assess the relative importance of the forcing-induced variability (climate change signal), and to characterize the various sources of uncertainty.

The rest of this paper is organized as follows: The data sets and methodologies are briefly described in sections 2 and 3, respectively. The estimates of climate changes projected by the three climate models combined are presented in section 4. The relative importance of forcing-induced variability and the various sources of uncertainty in the wave height climate change projections are discussed in sections 5 and 6, subsequently. This study is completed with a summary in section 7.

2. DATASETS

It has been shown that, on the seasonal time scale, significant wave height (SWH) variations in the northern hemisphere oceans over the past four decades are closely associated with contemporaneous mean sea level pressure (SLP) variations in the region (Wang and Swail 2002 and 2001). Such relationships between SWH and SLP fields have been used to make projections of SWH climate change scenarios for the 21st century (Wang et al. 2004a, Wang and Swail 2004). The same “downscaling” approach as in Wang et al. (2004a) was adopted in this study. The observed SLP-SWH relationships in each season were represented by a pair of regression models, one for seasonal means of SWH, another for the seasonal extremes of SWH. Thus, observations of seasonal mean SLP, and of seasonal means and maxima of SWH are needed to train the regression models. Both the observed SLP and SWH data used in this study were derived from the ERA-40 reanalysis for 1958-2001 (Gibson 2000, Gibson et al. 1996): Seasonal means and maxima of SWH were derived from the ERA-40 wave data (Caires et al. 2004), which are available at 6-hourly intervals on a 1.5°-by-1.5° lat/long grid over the globe. Similarly, monthly and seasonal mean SLP fields were derived from the 6-hourly SLP of the ERA-40, which are on a global 2.5°-by-2.5° lat/long grid. Then, the squared gradients of monthly mean SLP were also calculated from monthly means of SLP, and subsequently seasonally averaged. All the observed data (seasonal mean and maximal SWH, seasonal mean SLP and squared SLP gradient indices) were then re-expressed as anomalies relative to their 1961-1990 baseline climates, which in turn, were used as predictors when training the regression models.

Projections of future SLP anomalies were obtained from three coupled AOGCMs simulations for the IS92a, A2, and B2 forcing scenarios. The three climate models are: the Canadian CGCM2 (Flato and Boer, 2001), the Hadley Centre's HadCM3 (Gordon et al. 2000), and the German ECHAM4 (Roeckner et al. 1996a and 1996b). For each of the three forcing scenarios (i.e., IS92a, A2, and B2), three integrations with the same forcing but different initial conditions were run with the CGCM2, but only one integration was run with each of the other two models. All the A2 and B2 scenarios simulations cover the period 1990-2100. The IS92a scenario simulations with the CGCM2 and the HadCM3 cover the period 1900-2100, but with the ECHAM4 it covers the period 1860-2049.

The observations and projections of SLP fields, which are originally on different grids, were all converted to a global 96-by-48 Gaussian grid (approximately 3.75°-latitude by 3.75°-longitude) used by the CGCM2.

The AOGCMs simulated baseline (1961-1990) climate was calculated from the corresponding IS92a scenario simulations and subtracted from the relevant simulations of seasonal mean SLP to obtain anomalies of seasonal mean SLP simulated for each forcing scenario. The simulated SLP squared gradient indices were obtained from the simulated monthly means of SLP that were adjusted to the observed baseline climate (by replacing the simulated baseline climate with the observed baseline climate as derived from the ERA-40). The simulated anomalies of seasonal mean SLP and squared SLP gradient indices were then used as predictors in the SLP-SWH regression relationships to make projections of future seasonal means and extremes of SWH (see section 3 below).

3. METHODOLOGIES

3.1 Regression and non-stationary Generalized Extreme Value (GEV) analyses

As mentioned before, projections of SWH are based on the observed SLP-SWH relationships, which are represented by regression models in this study. Since we are dealing with both seasonal means and extremes of SWH (Gaussian and non-Gaussian variables), both conventional and generalized regression models were used here to represent the observed SLP-SWH relationship.

For the seasonal means, which are basically Gaussian distributed, the following regression model was fitted:

$$h_t = a + bP_t + cG_t \quad (1)$$

where h_t denotes the time series of seasonal mean SWH anomaly at a wave gridpoint, P_t and G_t are the time series of seasonal mean SLP anomaly and squared SLP gradient index at the wave gridpoint, respectively. Note that the SLP quantities (P_t and G_t), which are required on the fine wave grid, were calculated from values at four nearest SLP gridpoints (all within about 500 km radius from the wave gridpoint), using weights proportional to the inverse of the

distance. Here, P_t contains information about the mean state of SLP at time t , and G_t contains information about its variation in space, over the area within 500 km radius from the wave gridpoint (Wang et al. 2004a).

For each wave gridpoint, model (1) was trained using the time series h_t , P_t , and G_t derived from the ERA-40 wave and SLP fields. The statistical significance of the regression parameter b or c (which represents the relationship between the predictand h_t and the predictor P_t or G_t) was determined by performing likelihood ratio tests, in which the sum of squared errors (SSE) of the full model (1) was compared with the SSE of the one-predictor model that excludes the predictor being tested (i.e., $h_t = a + cG_t$ for the significance of b , and $h_t = a + bP_t$ for that of c ; Johnson and Wichern 1982). The result show that variation of seasonal mean SWH is closely related to both predictors P_t and G_t . Therefore, time series of P_t and G_t derived from the climate model simulations were substituted into the fitted model (1), i.e.,

$$\hat{h}_t = \hat{a} + \hat{b}P_t + \hat{c}G_t, \quad (2)$$

to make projections of seasonal mean SWH anomalies (h_t) for the period of 1990-2099 (1990-2049 for the ECHAM4 IS92a scenario) (\hat{y} denotes an estimate of y here and throughout this study).

Since non-Gaussian behaviour is a particular concern for extremes, and extremes from the changing climate system are most likely those of a non-stationary process, the non-stationary GEV analysis as described in Wang et al. (2004a) was carried out in this study to represent the relationship between seasonal extremes of SWH and the predictors P_t and G_t , and hence to make projections of future extreme wave heights. Specifically, the following five nested GEV models were fitted to the observed seasonal maxima of SWH (derived from the ERA-40 wave data) at each wave gridpoint:

$$GEV_0(\mathbf{m}, \mathbf{s}, \mathbf{x}) \quad (3)$$

$$GEV_1(\mathbf{m}_t = \mathbf{m}_0 + u_1 P_t, \mathbf{s}, \mathbf{x}) \quad (4)$$

$$GEV_2(\mathbf{m}_t = \mathbf{m}_0 + u_1 P_t + u_2 G_t, \mathbf{s}, \mathbf{x}) \quad (5)$$

$$GEV_3(\mathbf{m}_t = \mathbf{m}_0 + u_1 P_t + u_2 G_t, \log(\mathbf{s}_t) = b_0 + b_1 P_t, \mathbf{x}) \quad (6)$$

$$GEV_3(\mathbf{m}_t = \mathbf{m}_0 + u_1 P_t + u_2 G_t, \log(\mathbf{s}_t) = b_0 + b_1 P_t + b_2 G_t, \mathbf{x}). \quad (7)$$

The statistical significance of the linear relationships built in the GEV models (and the goodness of fit of the GEV models themselves) was assessed by performing likelihood ratio tests (see Wang et al. 2004a for the details). Consistent with what was reported by Wang et al. (2004a) and Wang and Swail (2004), results of the tests show that the location parameter is significantly correlated with both predictors P_t and G_t , but the scale parameter appears to be independent of them. In other words, the above GEV_2 is the model of best fit and was hence used to make projections of SWH extremes. Specifically, time series of P_t and G_t derived from the climate model simulations were substituted into the fitted expression for the location parameter to produce time series of the location parameter estimates for the period of 1990-2099 (1990-2049 for the ECHAM4 IS92a scenario), that is,

$$\hat{\mathbf{m}}_t = \hat{\mathbf{m}}_0 + \hat{u}_1 P_t + \hat{u}_2 G_t. \quad (8)$$

Such time series were then substituted into the fitted $GEV_2(\hat{\mathbf{m}}_t = \hat{\mathbf{m}}_0 + \hat{u}_1 P_t + \hat{u}_2 G_t, \hat{\mathbf{s}}, \hat{\mathbf{x}})$ to estimate possible future 20-yr return values of SWH, which were then subject to the Analysis of Variance to assess the relative importance of the forcing-induced variability and to characterize the various sources of uncertainty related to these projections (see section 3.2 below). Besides, as in Wang et al. (2004a), the time series of the projected location parameter values was subject to a trend analysis; and the trend component was in turn used to estimate changes in the size or frequency of extreme SWH (see section 4 below).

Note that there are a total of 15 scenario simulations: one for each of the three forcing scenarios with each of the three climate models (3×3), plus two extra integrations for each of the three forcing scenarios with the CGCM2 (2×3). For each of the 15 simulations, the above projections was done for each of the four seasons separately, with the four seasons being defined as January-March (JFM), April-June (AMJ), July-September (JAS), and October-December (OND).

3.2 Analysis of Variance (ANOVA)

Since there are various sources of uncertainty in the generation of projections of wave height climate change information, it is necessary to characterize the various sources of uncertainty and to assess the relative importance of the forcing-induced variability. To this end, both the one- and two-way ANOVA models were used in this study.

Since ensembles of the CGCM2 simulations have been produced with the same projected forcing but with different initial conditions that lead to different evolutions of the internal natural variability, a better assessment of the relative importance of the model's projected climate change can be done with a one-way ANOVA model. Let Y_{ts} denote time series of SWH (means or extremes) projected by the CGCM2 with one of the three forcing scenarios (time $t = 1, 2, \dots, n$; simulation $s = 1, 2, \dots, S$ where $S = 3$, i.e., a 3-member ensemble). The following one-way ANOVA model (Zwiers et al. 2000, Huitson 1966) was used in this study to assess the relative importance of variations due to the prescribed forcing,

$$Y_{ts} = \mathbf{b}_t + \mathbf{e}_{ts} \quad (9)$$

where \mathbf{b}_t represents the effects of the prescribed forcing (which are common to all simulations with the same forcing scenario), and \mathbf{e}_{ts} represents internally generated variations specific to simulation s . Here, it is assumed that 1) \mathbf{b}_t values are independent and identically distributed (iid) Gaussian random variable with mean $\bar{\mathbf{b}}$ and variance \mathbf{s}_b^2 , 2) \mathbf{e}_{ts} values are iid Gaussian random variable with mean zero and variance \mathbf{s}_e^2 . Then, the total sum of squares of variable Y_{ts} ,

$$TSS_Y = \sum_t \sum_s (Y_{ts} - Y_{oo})^2 \quad (10)$$

can be partitioned into two statistically independent variance components:

$$TSS_Y = SSB_Y + SSE_Y \quad (11)$$

where

$$SSB_Y = S \sum_t (Y_{to} - Y_{oo})^2 = S(n-1)\hat{\mathbf{s}}_b^2 + (n-1)\hat{\mathbf{s}}_e^2, \quad (12)$$

$$SSE_Y = \sum_t \sum_s (Y_{ts} - Y_{to})^2 = n(S-1)\hat{\mathbf{s}}_e^2, \quad (13)$$

and a “o” is used to replace a subscript when an arithmetic average is taken over that index (this notation is used throughout this paper). The statistical significance of the forcing-induced variability can be assessed by comparing

$$F_B = \frac{SSB_Y / (n-1)}{SSE_Y / [n(S-1)]} \quad (14)$$

with the critical value $F_p[(n-1), n(S-1)]$, where $F_p[\mathbf{n}_1, \mathbf{n}_2]$ denotes the p -quantile of the F distribution with \mathbf{n}_1 and \mathbf{n}_2 degrees of freedom. And the proportion of the total variance in quantity Y_{ts} that is due to the effect of the prescribed forcing is estimated as

$$P_B = \left[SSB - \frac{n-1}{n(S-1)} SSE_Y \right] / TSS_Y. \quad (15)$$

Zwiers et al. (2000) have shown that the above ANOVA-based test for the forcing-induced variability is much more powerful than the test that compares control and ensemble variances.

Similarly, let X_{ijt} denote a time series of SWH (means or extremes) projected by model i with forcing scenario j ($i = 1, 2, \dots, m$; $j = 1, 2, \dots, q$; time $t = 1, 2, \dots, n$. In this study, $m = 3$, $q = 3$, and $n = 60$). Then, we used the following two-way ANOVA model (Huitson 1966, Wang and Zwiers 1999) to partition the total variance of X_{ijt} into four components:

$$X_{ijt} = \mathbf{w} + \mathbf{g}_i + \mathbf{q}_j + \mathbf{d}_{ij} + \mathbf{e}_{ijt} \quad (16)$$

where \mathbf{w} is the grand mean of X_{ijt} , \mathbf{g}_i is the effect of differences among the three climate models (model uncertainty), \mathbf{q}_j is the effect of differences among the three forcing scenarios (forcing uncertainty), \mathbf{d}_{ij} is the effect of differences in the climate models' response to differences in forcing conditions (interaction; model-forcing uncertainty), and \mathbf{e}_{ijt} is the effects of the internal variability and the common forcing (i.e., forcing conditions that are common to all the three scenarios). Then, the total sum of squares of variable X_{ijt} ,

$$TSS = \sum_i \sum_j \sum_t (X_{ijt} - X_{ooo})^2 \quad (17)$$

can be partitioned into four statistically independent variance components:

$$TSS = SSM + SSF + SSI + SSE \quad (18)$$

where

$$SSM = nq \sum_i (X_{ioo} - X_{ooo})^2, \quad (19)$$

$$SSF = nm \sum_j (X_{ojo} - X_{ooo})^2, \quad (20)$$

$$SSI = n \sum_i \sum_j (X_{ijo} - X_{ajo} - X_{ioo} + X_{ooo})^2, \quad (21)$$

$$SSE = \sum_i \sum_j \sum_t (X_{ijt} - X_{ijo})^2. \quad (22)$$

The statistical significance of the model uncertainty (relative to the effects of the common forcing and internal variability) can be assessed by comparing

$$F_M = \frac{SSM / (m-1)}{SSE / [mq(n-1)]} \quad (23)$$

with the critical value $F_p [(m-1), mq(n-1)]$. And an unbiased estimator of the proportion of the total variance in quantity X_{ijt} that is due to the effect of differences among climate models is

$$P_M = \left[\frac{SSM - \frac{(m-1)}{mq(n-1)} SSE}{TSS} \right] \quad (24)$$

Similarly, the statistical significance of the forcing uncertainty can be assessed by comparing

$$F_F = \frac{SSF / (q-1)}{SSE / [mq(n-1)]} \quad (25)$$

with the critical value $F_p [(q-1), mq(n-1)]$. And the proportion of the total variance in quantity X_{ijt} that is due to the effect of differences among the forcing scenarios is estimated as

$$P_F = \left[\frac{SSF - \frac{(q-1)}{mq(n-1)} SSE}{TSS} \right] \quad (26)$$

The statistical significance of the interaction effects d_{ij} can be assessed by comparing

$$F_I = \frac{SSI / [(m-1)(q-1)]}{SSE / [mq(n-1)]} \quad (27)$$

with the critical value $F_p [(m-1)(q-1), mq(n-1)]$. And the proportion of the total variance in quantity X_{ijt} that is due to the effect of differences among models' response to different forcing conditions is estimated as

$$P_I = \left[\frac{SSI - \frac{(m-1)(q-1)}{mq(n-1)} SSE}{TSS} \right] \quad (28)$$

The statistical significance of the total uncertainty ($g_i + q_j + d_{ij}$) can be assessed by comparing

$$F_{MFI} = \frac{(SSM + SSF + SSI) / (mq-1)}{SSE / [mq(n-1)]} \quad (29)$$

with the critical value $F_p [(mq-1), mq(n-1)]$. And the proportion of the total variance in quantity X_{ijt} that is due to the effect of the total uncertainty is estimated as

$$P_{MFI} = \left[\frac{(SSM + SSF + SSI) - \frac{(mq-1)}{mq(n-1)} SSE}{TSS} \right] \quad (30)$$

Note that, in the above two-way ANOVA, only one of the three integrations for the same forcing scenario with the CGCM2 was used, because only one simulation was made with the other two models (HadCM3 and ECHAM4).

4. PROJECTED CHANGES IN OCEAN WAVE HEIGHTS

First of all, for either the A2 or the B2 forcing scenario, the three time series of seasonal mean (or extreme) SWH projected with the three climate models were combined into a single time series with three projected values for each year, to estimate the "mean" climate change projected by the three climate models. Since the changes were identified to be non-linear, the differences between the year 2080's and the year 1990's SWH were used to show the changes from year 1990 to year 2080, as in Wang et al. (2004a) and Wang and Swail (2004).

For the seasonal means of SWH projected with the A2 forcing scenario, as shown in Fig. 1, the areas of large increases in the North Pacific (NP) and the North Atlantic (NA) are similar to what was reported by Wang and Swail (2004) using only the CGCM2 projections for winter and fall. In the northern winter (JFM), the projected changes are characterized by significant increases in the mid-latitudes of the eastern NP and high-latitudes of western NP, as well as in the northeast Atlantic and in the southwest NA (off the southeastern coast of the United States). In the northern spring (AMJ) and summer (JAS), significant increases in seasonal mean wave heights were projected for the northeast

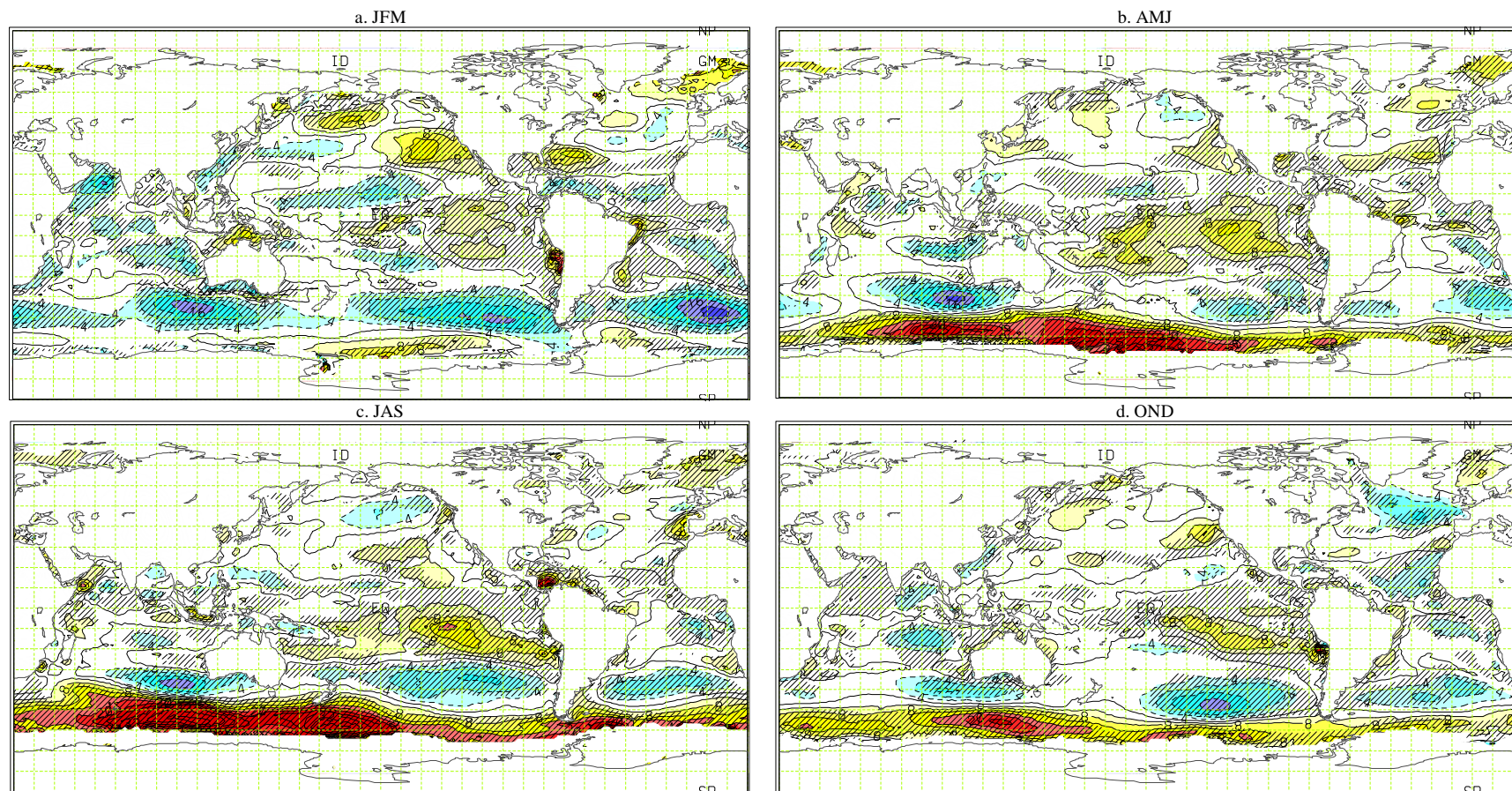


Fig. 1. Changes in the indicated seasonal mean SWH from 1990 to 2080 (2080's minus 1990's), as estimated from combining the three climate models' A2 scenario projections. The contour interval is 4 cm. Dashed and solid lines indicate negative and non-negative contours, respectively. Hatching indicates areas of significant (at 5% level) linear/quadratic trends in the projected seasonal means of SWH.

Atlantic, with some increases in the subtropical eastern NA and in the mid-latitudes of the eastern NP (Figs. 1b and 1c). In the northern fall (OND) season, the pattern of projected changes (Fig. 1d) is also similar to that shown in Wang and Swail (2004); however, changes projected by the three models combined are much smaller than those projected by the CGCM2 alone.

In the southern hemisphere, the changes projected for the JFM mean SWH are characterized by significant decreases in the region between 40°S and 60°S and some increases along the Antarctic coast (Fig. 1a). In the other three seasons, the projected changes are characterized by large increases in the region just off the Antarctic coast and some increases in the subtropical South Pacific (SP), with some decreases in the region between 40°S and 60°S (Figs. 1b-d).

With the weaker B2 forcing scenario, as shown in Fig. 2, the projected changes are generally smaller but have patterns similar to those projected with the A2 scenario, especially in the AMJ and JAS seasons. The biggest differences between the A2 and the B2 scenarios are seen in the southern hemisphere in OND (see Figs. 1d and 2b). However, there is little difference between the two scenarios in the regions off both the Atlantic and the Pacific coasts of the United States in winter (see Figs. 1a and 2a).

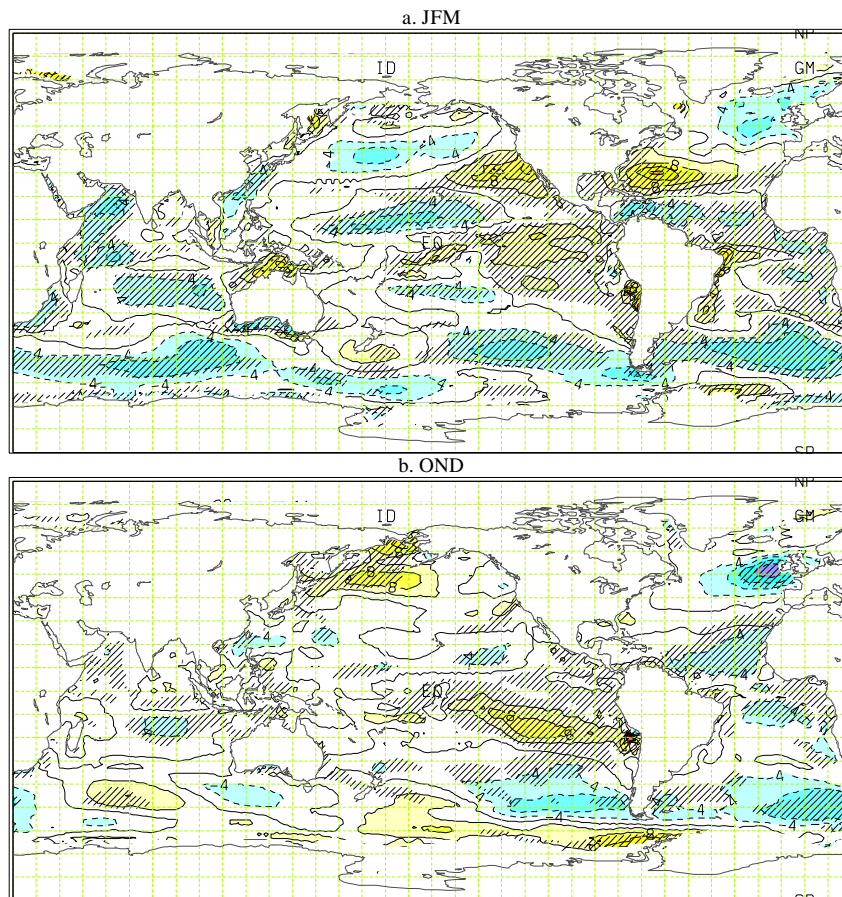


Fig. 2. The same as in Fig. 1 but for changes in the indicated seasonal mean SWH from 1990 to 2080 (2080's minus 1990's), as estimated from combining the three climate models' B2 scenario projections.

For the seasonal extremes, as shown in Figs. 3 and 4, the patterns of projected changes are also similar to, but not as smooth as their seasonal mean counterparts. The areas of statistically significant changes are not as extensive either. Again, the weaker B2 forcing scenario is generally associated with smaller changes than the A2 scenario. The JFM changes are characterized by increases in the regions off both the Atlantic and the Pacific coasts of the United States in winter, with the B2 forcing scenario being associated with slightly larger increases in the region off the Atlantic coast of United States. With the A2 forcing scenario, increases were also projected in the northeast Atlantic in all seasons, being largest in the JAS season. In the southern hemisphere, significant increases in seasonal extremes of SWH were projected for the region off the Antarctic coast in the AMJ and JAS seasons, with decreases in the region between 40°S and 60°S (cf. Fig. 3b-c). Such a pattern of changes was also projected for the OND season with the A2 forcing scenario (Fig. 4b).

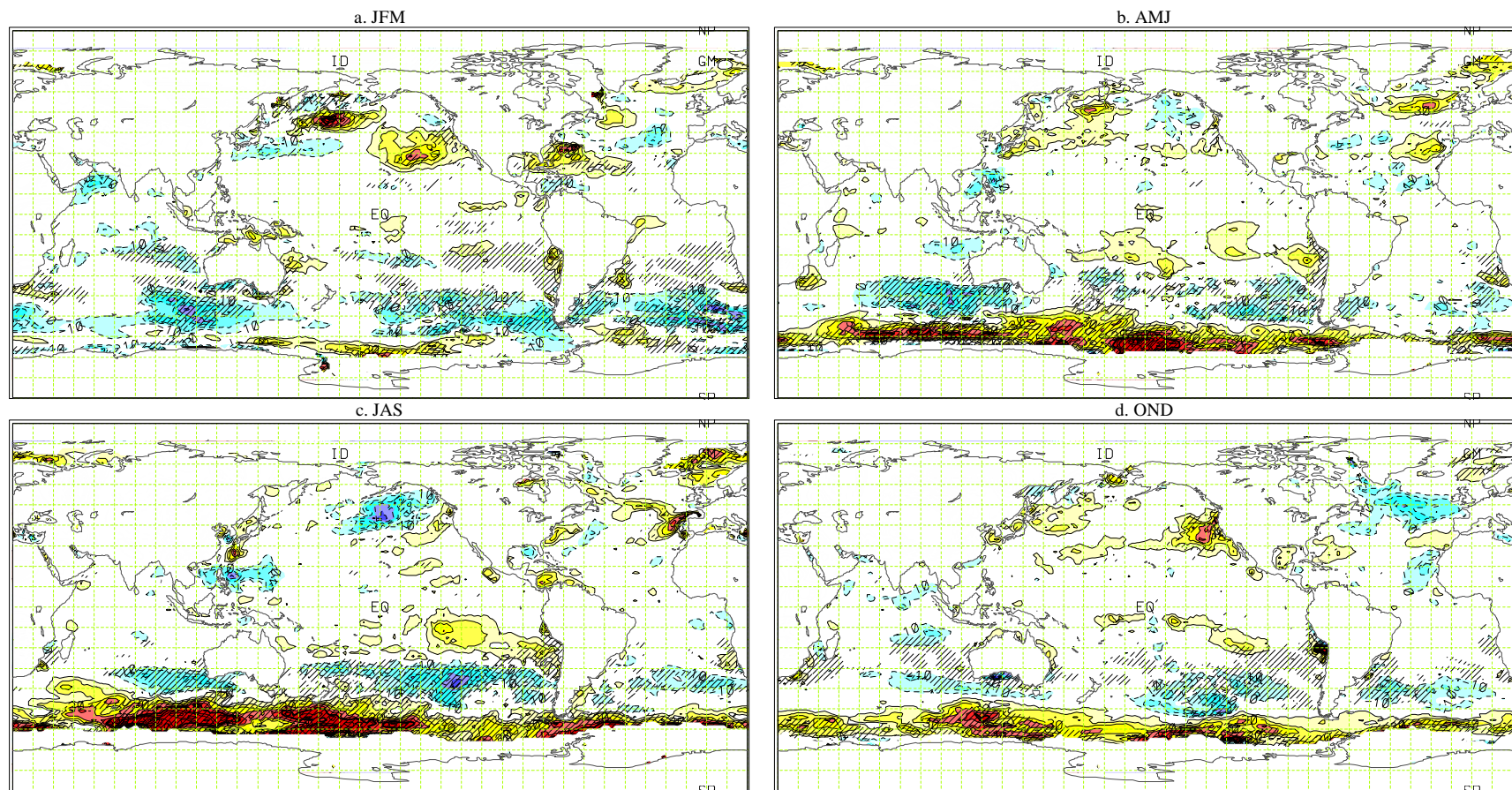


Fig. 3. Changes in the indicated seasonal 20-yr return values of SWH from 1990 to 2080 (2080's minus 1990's), as estimated from combining the three climate models' A2 scenario projections. The contour interval is 10 cm. Zero-contours are not drawn. Dashed and solid lines indicate negative and positive contours, respectively. Hatching indicates areas of significant (at 5% level) linear/quadratic trends in the projected location parameter of seasonal extreme SWH.

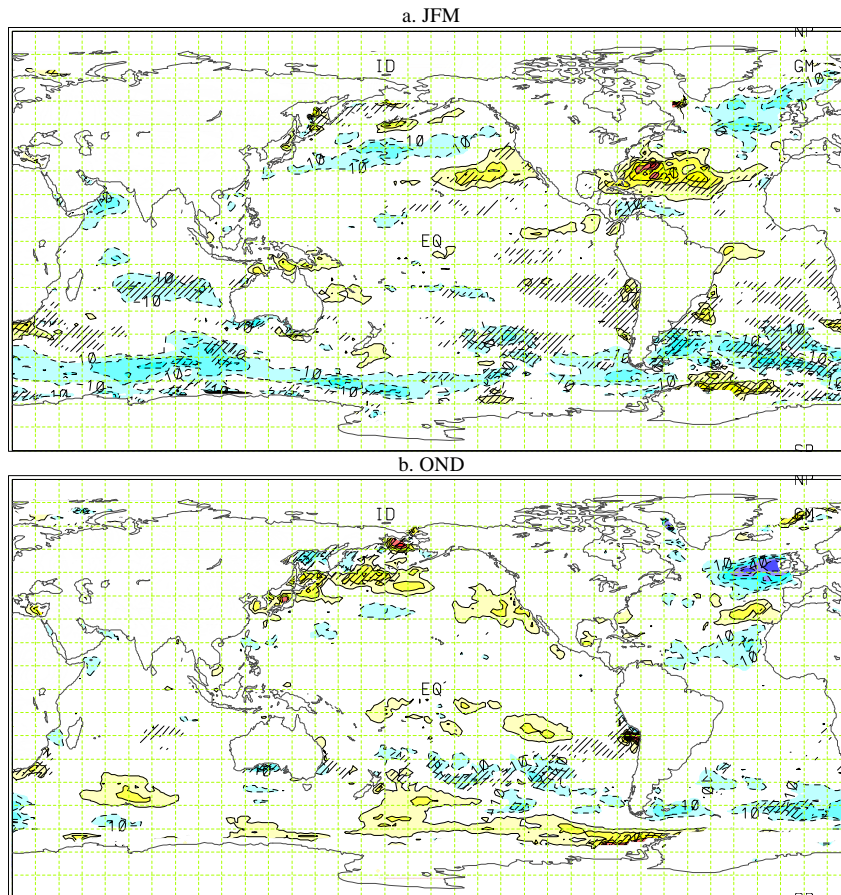


Fig. 4. The same as in Fig. 3 but for changes in the indicated seasonal 20-yr return values of SWH from 1990 to 2080 (2080's minus 1990's), as estimated from combining the three climate models' B2 scenario projections.

These projected changes in wave heights are consistent with the projected changes in extra-tropical storm tracks and cyclone activities (Wang et al. 2004b). The areas of significant increases in ocean wave heights were identified to have more frequent occurrence of strong cyclones in the projected warmer climate, and those of decreases in wave heights, less frequent strong cyclone activity. This connection makes sense physically.

5. RELATIVE IMPORTANCE OF THE FORCING-INDUCED VARIABILITY

As mention before, for each of the three forcing scenarios, three integrations were conducted with the CGCM2 with different initial conditions. These 3-member ensemble simulations allow us to assess the relative importance of the variability that is due to the prescribed forcing (climate change signal), by means of a one-way ANOVA. Thus, the one-way ANOVA as described in section 3.2 was applied to the A2 and B2 ensemble simulations, separately. Figure 5 shows the proportion of the total variance in the CGCM2 projected seasonal mean SWH that is due to the forcing prescribed in the A2 scenario. In winter, the forcing-induced variability is largest and most significant in the mid-latitudes of eastern NP, and in the tropical NP and the tropical NA (Fig. 5a). In the other three seasons, the largest proportions of forcing-induced variance are also seen in the NP, with the center of high proportions shifting westward to the central NP (Figs. 5b-d). The forcing-induced variability was also identified to be statistically significant in the region between 40°S and 60°S and in the tropical South Atlantic (SA) in all seasons, and also in the northeast Atlantic in the OND season (Fig. 5d). For the weaker B2 scenario, patterns of the forcing-induced variance proportions are quite similar to those shown in Fig. 5 and hence are not shown, but the proportions are generally smaller (e.g., about a half of those shown in Fig. 5a in the mid-latitudes of eastern NP), and the areas of significant forcing-induced variability are less extensive.

For the projections of seasonal extremes, the patterns of forcing-induced variability and the forcing-induced variance proportions are similar to those identified in the projections of seasonal mean SWH (cf. Figs. 5 and 6). The largest

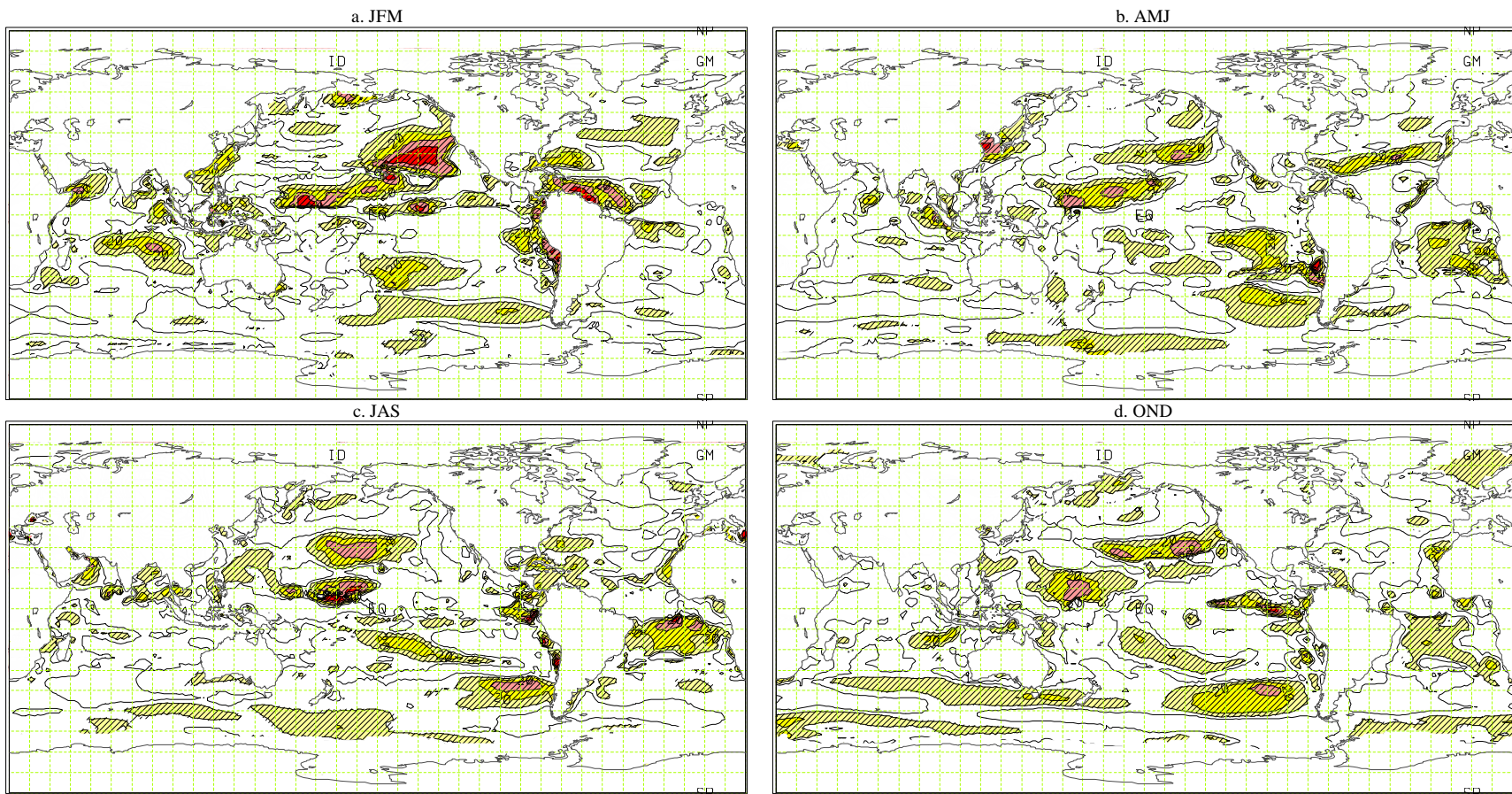


Fig. 5. The proportion of the total variance in the CGCM2 projected seasonal mean SWH that is due to the forcing conditions prescribed in the A2 scenario. The contour interval is 10%. Hatching indicates areas of statistically significant forcing-induced variability.

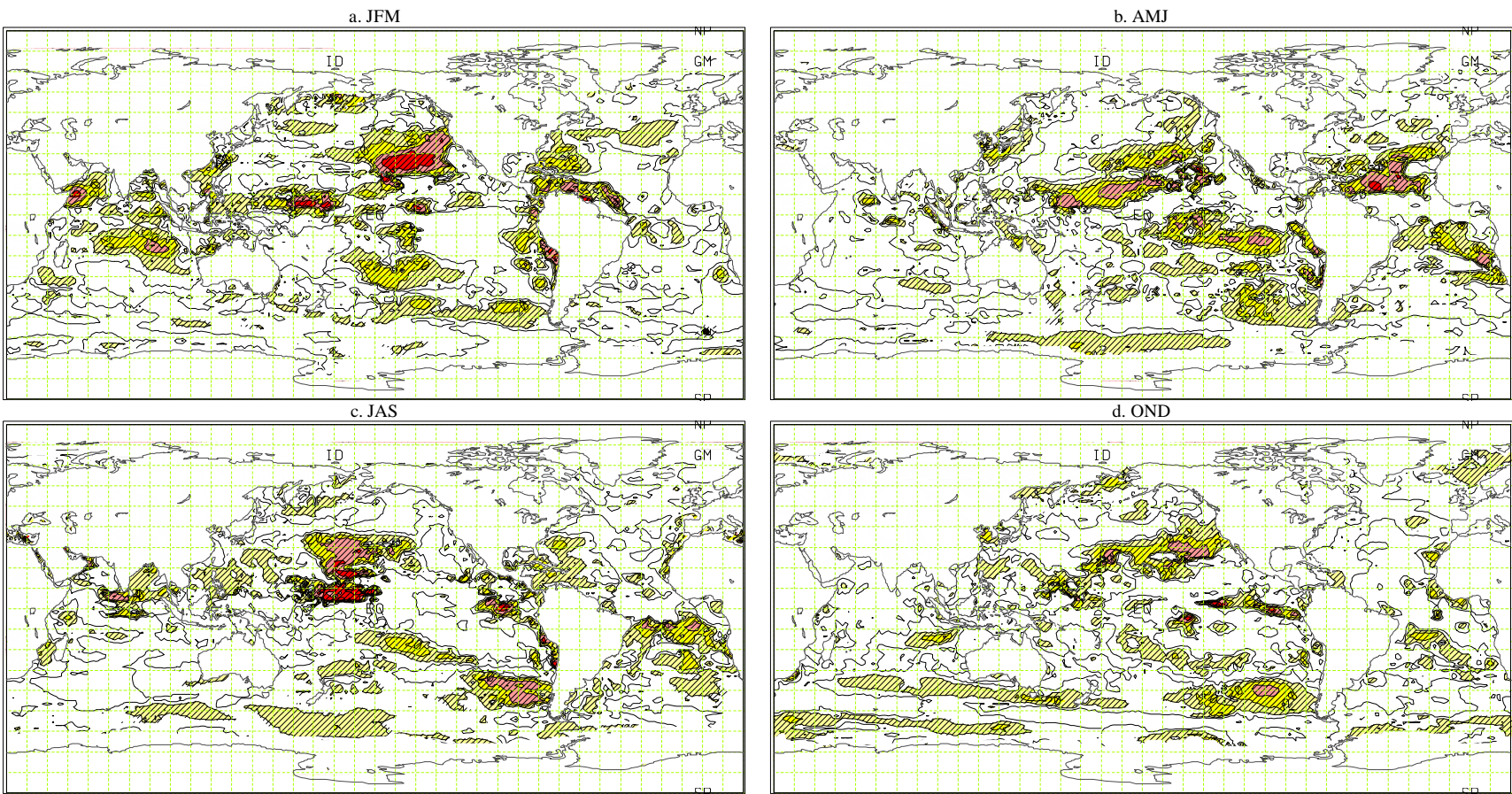


Fig. 6. The same as in Fig. 5 but the proportion of the total variance in the CGCM2 projected seasonal 20-yr return values of SWH that is due to the forcing conditions prescribed in the A2 scenario.

differences are seen in the AMJ season in the subtropical NP and subtropical NA, where the forcing appears to induce larger variability in the seasonal extremes than the seasonal means (see Figs. 5b and 6b).

Note that, with an ensemble size of 3, the forcing-induced variability has about 75% likelihood to be identified as statistically significant at 5% level when its variance proportion is 20%, and the likelihood reduces to about 30% when the variance proportion is 10% (Zwiers et al. 2000). So, an ensemble size of 3 is not ideal here. However, significant forcing-induced variability was identified, although it may have been underestimated.

6. CHARACTERISTICS OF THE VARIOUS SOURCES OF UNCERTAINTY

Remember that, for each of the three forcing scenarios, one simulation was performed with each of the three climate models. Thus, there are a total of 9 projections of seasonal mean (or extreme) SWH for the period of 1990-2049 (because the ECHAM4 IS92a projection covers only up to 2049). These projections can be classified into a 3-by-3 table for a two-way ANOVA, according to the three climate models (the “model effect”) and the three forcing scenarios (the “forcing effect”). This allows for the two-way ANOVA described in section 3.2, which was carried out for each of the four seasons, and for the seasonal means and extremes of SWH, separately. As a result, the proportions of the total variance in the projected SWH (means or extremes) that is due to either the “model effect” or the “forcing effect” or both of them, and their statistical significance, were estimated.

Figure 7 shows the proportion of the total variance in the projected JFM seasonal 20-yr return values of SWH that is due to the three sources of uncertainty: 1) uncertainty due to differences among the three climate models (i.e., model uncertainty or model effect); 2) uncertainty due to the differences among the three forcing scenarios (i.e., forcing uncertainty or forcing effect); 3) uncertainty due to different models’ responses to differences in forcing conditions (i.e., interaction or model-forcing uncertainty). Clearly, among the three sources of uncertainty, the model uncertainty is the largest, accounting for up to 50% of the total variance in the tropical Pacific; it dominates the pattern of the total uncertainty (see Fig. 8a). The forcing uncertainty is the smallest. Its variance proportions rarely exceed 10%. The small forcing uncertainty is not surprising, because the differences among the three forcing scenarios are not big (the IS92a scenario is similar to the A2 scenario, only the B2 scenario is relatively weaker; see Wang et al. 2004a). It should be pointed out that the forcing uncertainty is statistically significant in most areas of the ocean, although it is small in general. This means that different forcing conditions do make significant differences in the projections of ocean wave heights.

In the other seasons, the situation is similar. The uncertainty of wave climate change projections is also mainly due to differences among the three climate models. Thus, only the total uncertainty is shown in Fig. 8. Clearly, among the four seasons, the total uncertainty is smaller in the northern winter (JFM) and spring (AMJ) than in the other two seasons. Generally, the uncertainty is small in the middle-high latitudes, especially in the northern winter and spring (Fig. 8a-b); but it is large in the tropics (Fig. 8).

For the projections of seasonal mean SWH, the three sources of uncertainty, and the total uncertainty, have characteristics that are quite similar to those shown in Figs. 7-8, in terms of both the pattern and the magnitude (and hence are not shown here). Again, the uncertainty mainly arises from the differences among the three climate models. The forcing uncertainty is also statistically significant, although it is much smaller than the model uncertainty.

7. SUMMARY

In this study, we have made and analyzed projections of seasonal means and extremes of ocean wave heights using projections of possible future climates conducted with three global climate models for three forcing scenarios. We have estimated the multiple-model-mean climate change by combining the three climate models’ projections for the same forcing scenario. We have assessed the relative importance of the variability in the projected wave heights that is due to the forcing prescribed in the A2 or B2 scenario, using the CGCM2 ensemble simulations. We have also characterized the uncertainty in the wave height climate change projections that is due to differences among the three climate models and/or differences among the three forcing scenarios.

The results show that the multiple-model-mean climate change has patterns similar to those derived from using the CGCM2 projections alone, but the magnitudes of changes are generally smaller. Statistically significant forcing-induced variability was identified in some areas in all four seasons, being largest in the NP in the JFM season with the A2 forcing scenario, although it may be underestimated due to the limited ensemble size of 3. The uncertainty in the projections of wave height climate change is mainly due to differences among the climate models; and it is smaller in the JFM and AMJ seasons than in the JAS and OND seasons. Note that the uncertainty is generally small in the mid-high latitudes. In particular, the areas of large projected changes (e.g. the mid-latitudes of eastern NP) were identified to have very small uncertainty (cf. Figs. 5a and 8a). Also, the forcing uncertainty was identified to be statistically

significant in most areas of the oceans, although it is small relative to the model uncertainty. This indicates that different forcing conditions do make significant differences in the wave height climate change projection.

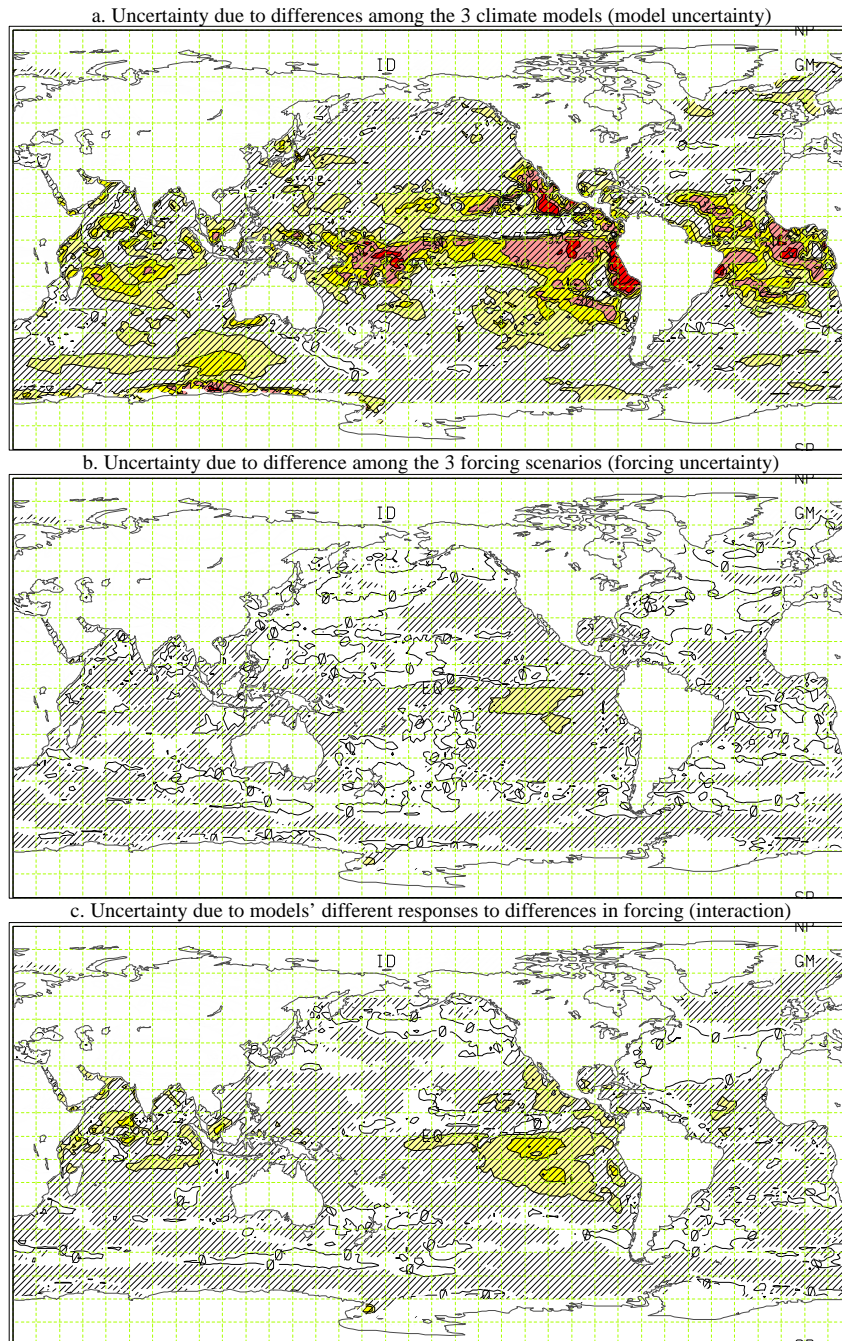


Fig. 7. The proportion of the total variance in the projected JFM seasonal 20-yr return values of SWH that is due to the effects of the indicate uncertainty. The contour interval is 10%. Hatching indicates areas of statistically significant (at 5% level) uncertainty.

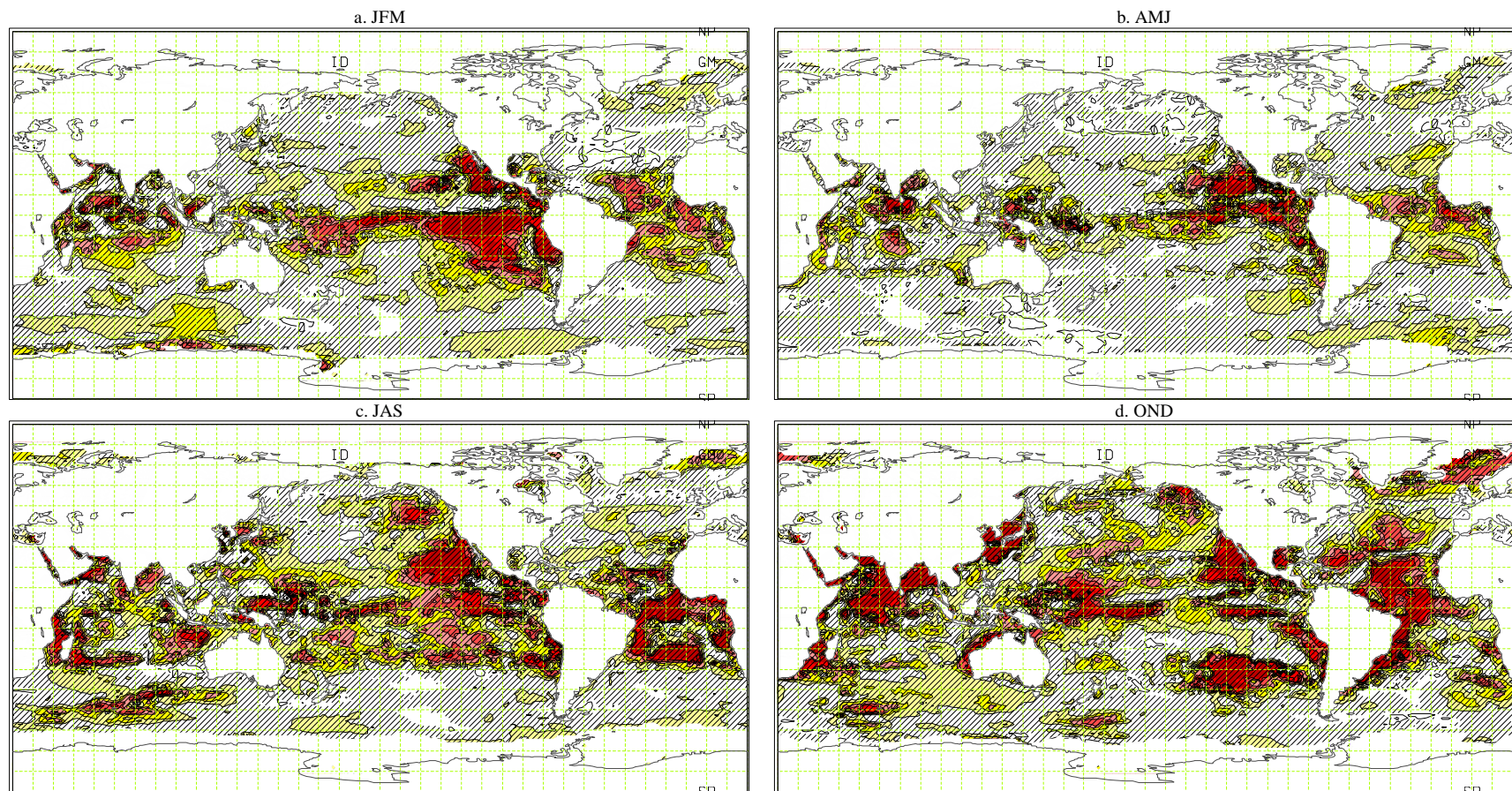


Fig. 8. The proportion of the total variance in the projected seasonal 20-yr return values of SWH that is due to the effect of the total uncertainty. The contour interval is 10%. Hatching indicates areas of statistically significant (at 5% level) uncertainty.

8. ACKNOWLEDGMENTS

The authors are greatly indebted to Qiuzi Wen and Yang Feng for their computing support.

9. REFERENCES

- Caires, S., A. Stearl, G. Komen, and V. Swail, 2004: The Web-based KNMI/ERA-40 global wave climatology atlas. *WMO Bulletin*, **53**(2), 142-146.
- Flato, G. M. and G. J. Boer, 2001: Warming Asymmetry in Climate Change Simulations. *Geophys. Res. Letters*, **28**, 195-198.
- Gibson, R., P. Kallberg, and S. Uppala, 1996: The ECMWF Reanalysis (ERA) Project. *ECMWF Newsletter*, **73**, 7-17.
- Gordon, C., C. Cooper, C.A. Senior, H. Banks, J.M. Gregory, T.C. Johns, J.F.B. Mitchell and R.A. Wood, 2000: The simulation of SST, sea ice extents and ocean heat transports in a version of the Hadley Centre coupled model without flux adjustments. *Climate Dynamics*, **16**(No. 2-3), 147-168.
- Houghton, J.T., Y. Ding, D.J. Griggs, M. Noguer, P.J. van der Linden, X. Dai, K. Maskell, and C.A. Johnson, Eds., 2001: Climate Change 2001: *The Scientific Basis. Contribution of Working Group I to the Third Assessment Report of the Intergovernmental Panel on Climate Change*. Cambridge University Press, 881pp.
- Huitson, A., 1966: *The Analysis of Variance*. Charles Griffin & Company Ltd., London.
- Johnson, R. A. and D. W. Wichern, 1982: *Applied Multivariate Statistical Analysis*. Prentice-Hall, Inc., Englewood Cliffs, New Jersey, USA, 594pp.
- Nakicenovic, N., and R. Swart, Eds., 2000: *Special Report on Emissions Scenarios (SRES)*. Cambridge University Press, 599pp.
- Roeckner, E., K. Arpe, L. Bengtsson, M. Christoph, M. Claussen, L. Dmenil, M. Esch, M. Giorgetta, U. Schlese, U. Schulzweida, 1996a: The atmospheric general circulation model ECHAM-4: Model description and simulation of present-day climate. *Report No. 218 of the Max-Planck Institute for Meteorology*, Hamburg, Germany.
- Roeckner, E., J.M. Oberhuber, A Bacher, M. Christoph, and I. Kirchner, 1996b: ENSO variability and atmospheric response in a global coupled atmosphere-ocean GCM. *Climate Dynamics*, **12**, 737-754.
- Simmons, A. J. and J. K. Gibson, 2000: The ERA-40 Project Plan. ERA-40 Project Report Series No. 1. [Available online at <http://www.ecmwf.int/research/era/>.]
- Wang, X. L., F. W. Zwiers, and V. R. Swail, 2004a: North Atlantic Ocean Wave Climate Change Scenarios for the Twenty-First Century. *J. Climate*, **17**, 2368-2383.
- Wang, X. L., V. R. Swail, and F. W. Zwiers, 2004b: Changes in extra-tropical storm tracks and cyclone activities as derived from two global reanalyses and the CGCM2 projections of future climate. Manuscript to be submitted to *J. Climate* soon (also in this Volume of reprints)
- Wang, X. L., and V. R. Swail, 2004: Historical and possible future changes of wave heights in northern hemisphere oceans. *Atmosphere Ocean Interactions - Volume 2* (Ed.: W. Perrie), Wessex Institute of Technology Press (in press).
- Wang, X. L. and V. R. Swail, 2002: Trends of Atlantic wave extremes as simulated in a 40-year wave hindcast using kinematically reanalyzed wind fields. *J. Climate*, **15**(9), 1020-1035.
- Wang, X. L. and V. R. Swail, 2001: Changes of Extreme Wave Heights in Northern Hemisphere Oceans and Related Atmospheric Circulation Regimes. *J. Climate*, **14**, 2204-2221.
- Wang, X. L. and F. W. Zwiers, 1999: Interannual Variability of Precipitation in an Ensemble of AMIP Climate Simulations Conducted with the CCC GCM2. *J. Climate*, **12**, 1322-1335.
- Zwiers, F. W., X. L. Wang, and J. Sheng, 2000: Effects of specifying bottom boundary conditions in an ensemble of atmospheric GCM simulations. *J. Geophys. Res.*, **105**(6), 7295-7315.